

Article

Assessing Sea Surface Temperatures Estimated from Fused Infrared and Microwave Data

Jinyang Ni ¹, Jiajun Feng ¹ , Runxia Sun ¹ and Yuanzhi Zhang ^{1,2,*}¹ School of Marine Sciences, Nanjing University of Information Science and Technology, Nanjing 210044, China² Department of Geography and Resource Management, Faculty of Social Science, Chinese University of Hong Kong, Shatin, Hong Kong

* Correspondence: yuanzhizhang@cuhk.edu.hk or yzhang209@nuist.edu.cn; Tel.: +852-6995-2064

Abstract: Sea surface temperature (SST), a critical parameter of the global ocean–atmosphere system, is an essential element in the study and in the application of marine science. Satellite–infrared observations currently represent the only available method for continuous, large-scale observation of SST. Although passive microwave observations are not blocked by clouds, allowing for data collection in all weather conditions, this technological tool is characterized by low spatial resolution. Conversely, infrared observations offer high resolution but are susceptible to cloud obscuration. Accordingly, a technique that effectively fuses microwave and infrared satellite observations into a high-resolution SST field with global coverage close to the actual distribution is of practical significance. This paper describes fusing MODIS infrared remote sensing and AMSR-2 microwave remote sensing SST data with an optimal interpolation (OI) approach to produce a high-resolution SST data. The study chose the coastal Kuroshio region of China to establish an appropriate scale for examining the spatial structure of SST and attaining a more realistic picture of SST observations and impacts. The included discussion of the sources of error in the fusion process provides a reference for improving the accuracy of fused marine remote sensing data. The study also compared the fused SST results and the current international mainstream multi-temporal resolution of the three using the OI algorithm. We compared the fusion product with ARGO data with and without typhoon impact to explore and practice the OI in SST fusion when evaluating the accuracy of different data in the case of external disturbance being present. The research results have great significance for improving regional SST forecast accuracy while ensuring the applicability of various approaches to fusing SST data by incorporating the influence of typhoons in the offshore region of the East China Sea (ECS). Implications for the future development of SST fusion data are also included in the discussion.

Keywords: sea surface temperature; optimal interpolation; assimilation

Citation: Ni, J.; Feng, J.; Sun, R.; Zhang, Y. Assessing Sea Surface Temperatures Estimated from Fused Infrared and Microwave Data. *Water* **2022**, *14*, 3357. <https://doi.org/10.3390/w14213357>

Academic Editor: Zheng Duan

Received: 1 October 2022

Accepted: 20 October 2022

Published: 23 October 2022

Publisher's Note: MDPI stays neutral with regard to jurisdictional claims in published maps and institutional affiliations.



Copyright: © 2022 by the authors. Licensee MDPI, Basel, Switzerland. This article is an open access article distributed under the terms and conditions of the Creative Commons Attribution (CC BY) license (<https://creativecommons.org/licenses/by/4.0/>).

1. Introduction

The Earth has a surface area of 510 million km², 71% of which is covered by seawater. Due to the enormous specific heat capacity of seawater, the surface layer of the ocean stores most of the energy from solar radiation, and this stored heat essentially controls atmospheric motion. Along these lines, the energy sources that drive atmospheric motion include the sensible heat exchange between the sea surface and the atmosphere, the latent heat of seawater, and long-wave radiation. Heat exchange between the atmosphere and the ocean takes place primarily at the ocean's surface, where changes in thermal conditions impose corresponding changes in atmospheric movement. As a parameter that correlates to the thermal conditions of the ocean surface, sea surface temperature (SST) is frequently featured in studies examining upper ocean processes and sea–air heat exchange. SST is also widely used in numerical simulations and forecasts concerning the ocean and atmosphere. The results of sea–air interaction studies have indicated that changes in SST can have fundamental effects on long-term weather processes [1], leading to alteration in the marine

environment and global climate. In particular, SST conditions influence the development and production of marine fisheries in light of the specific temperature range required for growth by various oceanic fish species. Hence, accurate SST data are essential in effectively identifying the ideal location of central fishing grounds as well as assessing the development status of fishing grounds. SST also serves as a critical indicator for the regular assessment of established marine fisheries, whose production in terms of the growth of the fish cultured is heavily dependent on SST conditions. The availability of SST data is an integral part of forecasting fishing conditions. Lastly, SST is a factor in global climate change and is implicated in the occurrence of natural disasters, such as typhoons, and climate patterns, such as El Niño [2]. Accordingly, practical production applications require the ready availability of high-resolution spatial and temporal SST data with global coverage that supports the efforts to sensibly exploit the ocean, improve the efficiency of fishery production, and study marine science and global climate change.

The development of methods that will improve SST data accuracy has continued to draw increasing scholarly attention. Traditional in situ measurement data, such as information collected by ships and buoys, are constrained to ship routes and buoy positions, leaving wide stretches of ocean unmonitored and large blank areas on comprehensive SST charts. Compared with traditional observation methods, marine satellite remote sensing technology can cover wide range of ocean waters in all weather conditions over long periods of time, while reporting data nearly in real time [3]. In addition, satellites can periodically repeat observations for the same sea area. Although the many advantages of satellite remote sensing thus lend themselves to fishery production and marine research, it is also vital to recognize that different satellite sensors are accompanied by various disadvantages. For example, infrared sensors offer high spatial and temporal resolution but cannot penetrate the cloud layer to obtain data. Conversely, microwave radiometers can penetrate the cloud layer but cannot meet the requirement for production and research-related accuracy because of their low spatial resolution [4].

Advances in satellite observation technology have supported an increasing number of in-orbit observation satellites, fueling the growth of scholarly attention focused on methods that can combine the characteristics of different types of satellite data to achieve multi-source satellite SST data fusion. The leading data fusion methods currently include objective analysis, stepwise revision, variational assimilation, Kalman filter, and optimal interpolation (OI) [5]. The first application of an objective analysis method in the context of oceanographic research was conducted by Bretherton et al. in 1976 [6]. In 1987, Carter and Robinson [7] explained in detail and provided a methodology for assessing different flow fields using objective analysis, which the researchers specified as applicable to marine satellite remote sensing data. Reynolds and Smith [8] used the OI method to combine in situ measured SST data with satellite-observed SST data to obtain fused SST data. Reynolds further improved the OI fusion SST data method in 2002 [9], boosting the accuracy of the fused data in high latitudes. Around the same time, He et al. [10] used the OI method to fuse IR (AVHRR) and microwave (TMI) data in the Florida West Florida Shelf in 2003. Meanwhile, the European Commission's Joint Research Centre (JRC) established the GODAE High Resolution SST Pilot Project (GHRAAT-PP) [11] in 2000 and 2005. Most of the SST L4 products released by the GHRSSST-PP have used the OI method. Remote Sensing Systems (RSS) developed the microwave OI global SST analysis system [1], combining SST data from TMI, AMSR-E, and the Moderate-resolution Imaging Spectroradiometer (MODIS) on the Aqua satellite platform. Lastly, the National Centre for Ocean Forecasting (NCOF) developed the Operational Sea Surface Temperature and Sea Ice Analysis (OSTIA) system [12], which used OI to combine measured SST data with satellite SST data to obtain fused daily average SST data at a resolution of $1/20^\circ$.

In summary, many approaches to obtaining high-quality remote sensing SST data via the fusion of different types of SST data have been developed around the world. Among them, widely used offerings that provide high accuracy include the National Climate Data

Center's (NCDC) OISST v2 [13], the National Weather Service's RTG-HR and OSTIA, and the UK Meteorological Offices' OSTIA [12].

Most SST data analyses employ statistical analysis to transform irregular spatial data into regular grid products [14]. However, these methods generally exclude the effects on SST of extreme weather events, such as typhoons [15], leading to large local variations in day-by-day results. The differences in SST data based on the data collection technology, as mentioned earlier in this discussion, have led to the availability of many variations of SST data, each of which offers unique advantages to various research areas and fulfills different user requirements in terms of providing a particular solution that will best suit the established purpose. This investigation pursued several objectives. First, the study sought to verify the differences between single sensor data and the resulting spatially seamless daily SST values in the case study of the East China Sea (ECS). The second objective was to compare the differences between the measured data and the fused SST under the influence of typhoons. Therefore, we began by defining the study area using Argo measurements and then applied three typical global fusion SST data (AVRHH OISST, MISST, and OSITA), and MODIS and AMSR2 data (SST-OI) with different spatial resolutions. The research results have great significance for improving SST forecasting capability under the influence of regional typhoons while also supporting the effective application of various fused SST products in the ECS.

2. Study Area and Datasets

2.1. Study Area

The study area is the Kuroshio region in the East China Sea (15–45° N, 110–150° E), which is part of the northwest Pacific Ocean (as shown in Figure 1), influenced by a subtropical high pressure and monsoon system, with high typhoon occurrence, and the Kuroshio winding northward through the region, which is a complex and variable climate and hydrodynamic environment, making it an ideal sea area for accuracy testing of SST fusion products.

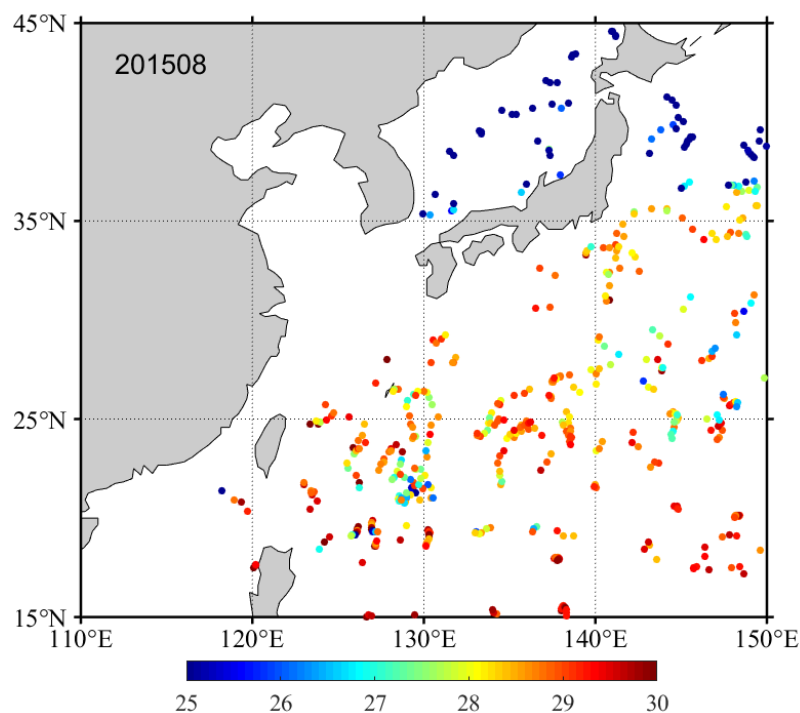


Figure 1. Study area, where the dots represent the location of the ARGO buoys (SST, colored shading; °C). The figure shows the overlay of daily ARGO buoy SST observation point locations in the study area in August 2015.

2.2. Fusion Satellite Datasets

The satellite SST data used in this fusion study include MODIS thermal infrared data and AMSR-2 radiometer microwave data. The MODIS data are from NASA's Jet Propulsion Laboratory (JPL), whose SST data have a spatial resolution of 0.041° , named NASA OBPG. 2020. MODIS Aqua Global Level 3 Mapped SST. Ver. 2019.0. These data are available through the website https://podaac.jpl.nasa.gov/dataset/MODIS_AQUA_L3_SST_THERMAL_DAILY_4KM_Daytime_V2019.0 (dataset accessed on 26 June 2022).

AMSR-2 SST data are provided by Remote Sensing Systems (RSS), named GHRSSST Level 3U Global Subskin Sea Surface Temperature version 8a from AMSR2 on the GCOM-W satellite, Ver. 8a. The product, with a spatial resolution of 0.25° , is available through the website <https://podaac.jpl.nasa.gov/dataset/AMSR2-REMSS-L3U-v8a> (dataset accessed on 26 June 2022).

This study uses MODIS SST data from January 1–3, 2015, for validation of OI method feasibility. AMSR-2 SST data of the same time and study area as MODIS were selected for this thesis study, allowing a final SST data fusion product with 9 km spatial resolution (to facilitate intercomparison among the fused SST products, see Section 3.1 for details) to be obtained. August is a time when typhoons are frequent in the study area, meaning we can conveniently compare the impact of typhoons on SST products. Therefore, the fusion product also uses data from August 2015, which is then compared with other products (see Section 4.2 for details).

2.3. In Situ Data and Typhoon Data

Among the various raw SST data sources, drifting buoys have been widely used to validate numerous satellite-derived SST data due to the measurement depths observed by satellite sensors close to the sea surface [16]. Although the measured depths of the drifting buoy and the satellite SST are slightly different, there is a strong correlation between the measured values of the drifting buoy and the satellite SST [17]. The Argo program is a global ocean observing program launched in 1998 to collect fast and accurate profiles of seawater temperature, salinity, and currents in the upper layers of the global ocean [18,19].

The Argo SST data adopted in this work were taken from the Coriolis Global Data Acquisition Center of France. The Argo program is part of the Global Ocean Observing System (GOOS) [20], covering the full month of August 2015 and the area of ECS. These data include delayed-mode profiles with a quality flag of 1. The Argo buoy returns a set of profiles every 10 days, and the shallowest water depth at which it collects temperatures is 4–5 m, with very little data in the 0-m layer. To obtain sufficient surface temperature information, the 0–5 m layer was selected as the validated surface measurements, following Marcello et al. [21]. Figure 1 illustrates the distribution of surface (0–5 m) depth Argo in the study area in August 2015.

To compare the differences among SST products under extreme conditions, this paper considers the effects of typhoons. The typhoon data sources were taken from the "CMA-STI Tropical Cyclone Best Track Dataset" [22,23], which includes the central location, minimum pressure, maximum wind speed, average speed, and duration of the typhoon (tcdata.typhoon.org.cn, accessed on 26 June 2022). The typhoon situation in the study area in August 2015 is detailed in Figure 2.

2.4. SST Datasets

Since the 1980s, the increasing number of satellite remote sensing SST data sources has greatly contributed to the development of specific algorithms for SST products, and a wide range of SST products have been developed by research institutes and operational departments around the world. Because the purposes of research can vary, the data sources selected for fusion production of each product vary from country to country, as do the fusion techniques used and the spatial and temporal resolution of the products.

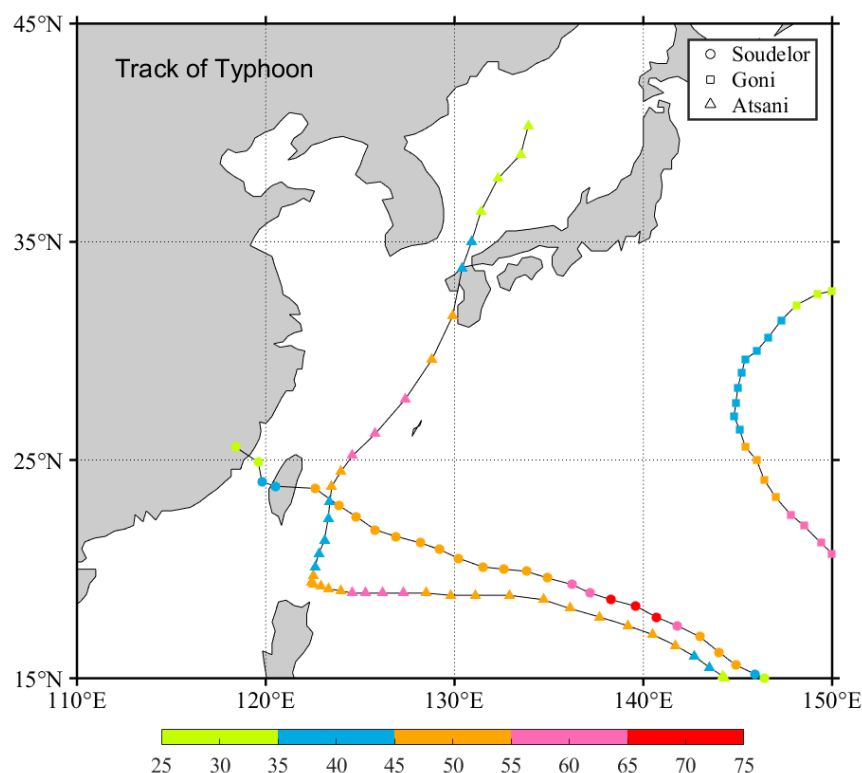


Figure 2. Typhoon track map for August in the study area (wind speed, colored shading; m/s). The circle represents Typhoon Soudelor (1–8 August, max radius of over 24 m/s winds 180 km), the square represents Goni (15–26 August, max radius of over 24 m/s winds 220 km), the triangle represents Atsani (16–26 August, max radius of over 24 m/s winds 240 km).

It is difficult to say with certainty that a particular fusion product produces the best effect. We can only choose the appropriate SST fusion product by combining it with actual demand.

The data sources of the SST analysis data used for comparison in this paper are three fusion data of the Advanced Very High Resolution Radiometer (AVHRR) NOAA OISST [13], Microwave + Infrared optimally interpolated SST (MISST) and Operational SST and sea ice analysis (OSTIA) [12].

The OISST data is a day-by-day SST product produced by Reynolds' team [24], including two fusion data, NOAA OISST and NOAA + AMSR OISST, with a spatial resolution of 0.25° [25]. Due to the failure of the AMSR-E satellite antenna, the NOAA + AMSR OISST product was discontinued on 5 October 2011. Here, the NOAA OISST, a Global Level 4 SST analysis data of the High Resolution Sea Surface Temperature Team (GHRSSST), is selected to use only AVHRR infrared data and measured data. It first corrects the large-scale bias generated by daytime remote sensing data using measured data, and then, using the OI, a smoothed complete field is obtained by interpolating and extrapolating SST observations from different sources. The fusion data is computationally generated.

The MISST data is the global daily grid SST value produced by RSS (Remote Sensing Systems), with a spatial resolution of 0.09° . MISST is based on the OI algorithm and incorporates microwave data that can penetrate clouds and infrared data with high spatial resolution. The data, using both microwave (MW) sensors including the Global Precipitation Measurement (GPM) Microwave Imager (GMI), the Tropical Rainfall Measuring Mission (TRMM) Microwave Imager (TMI), the NASA Advanced Microwave Scanning Radiometer-EOS (AMSRE), the Advanced Microwave Scanning Radiometer 2 (AMSR2), and WindSat, operates on the Coriolis satellite, and infrared (IR) sensors such as the MODIS on the NASA Aqua and Terra platform and the Visible Infrared Imaging Radiometer Suite (VIIRS).

OSTIA is produced and published daily by the Met Office of the UK Meteorological Office using the Optimal Interpolation Algorithm (OI) based on data provided by GHRSS-PP. OSTIA includes the use of satellite data from sensors that the AVHRR, the Advanced Along Track Scanning Radiometer (AATSR), the Spinning Enhanced Visible and Infrared Imager (SEVIRI), the Advanced Microwave Scanning Radiometer-EOS (AMSRE), the Tropical Rainfall Measuring Mission Microwave Imager (TMI), and in situ data from drifting and moored buoys. Its spatial resolution is 0.054° [1].

3. Methods

3.1. Fusion Method

The OI algorithm is one of the more practical and easily operationalized fusion algorithms for SST data fusion. Among the many SST products available today, the OI method is used in many mainstream SST fusion data [13,24], which shows the feasibility of the algorithm in marine research.

In order to get a better fusion effect, the selected SS data coverage should be as high as possible, since the data of one day alone often cannot reach the requirements. The MISST product determines the SST for one day in the middle of three consecutive days of remotely sensed observations by time smoothing. All daytime observations are adjusted and corrected by the wind speed at local time [1]. In this study, for MODIS and AMSR2 data to be fused, the SST data of three consecutive days are averaged to represent the SST of its second day, referring to the practice of MISST [1].

Since the spatial resolution of MODIS and AMSR-2 SST data are not the same, the fusion work cannot be performed directly. The two sets of data need to be geometrically transformed in the same coordinate system before fusing. In this thesis, a bilinear interpolation method is used to transform the data geometrically, and both sets of data are interpolated into a grid with a resolution of 9 km, i.e., the size of the grid points in the study area is 455×341 . Then the optimal interpolation method is applied to them.

The optimal interpolation [8] is an objective analysis method in which the background, observed and analyzed values are set as unbiased estimates, and the observed and analyzed values are expressed in the form of increments relative to the background values. Then the mean squared deviation is minimized by calculation, which is a linear interpolation method. In calculating the optimal interpolation, the deviation of the measured data from the background field is weighted and averaged to obtain the values of the spatial grid points. The flow of satellite SST data fusion is shown in Figure 3.

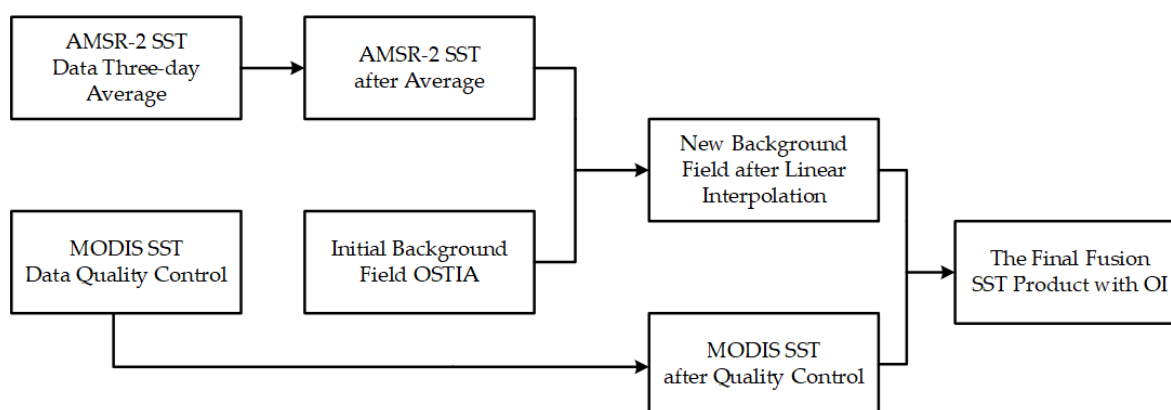


Figure 3. Fusion of MODIS and AMSR-2 SST data flow with the OI.

In order to improve the accuracy of the SST fusion product, only those parts of the MODIS satellite data with better quality markers are fused. The data analysis shows that the quality of MODIS data is affected by cloud occlusion, land, cloud edge, and solar flare. The IR radiometer can obtain high accuracy and reliable SST measurements in the area free of these effects. The quality marker distribution of MODIS data in the study area of this

paper, where only the grid points with flag = 0 are not disturbed, are valid data. The rest of the grid point data are regarded as invalid data.

3.2. Fusion SST Image Quality Analysis

The image is subjectively evaluated by comparing its visual effect, whereas objective evaluation calculates its statistical parameters [26,27]. The results of subjective evaluation depend on humans' visual observation, whereas the results of the objective evaluation are more impartial.

In this paper, to reflect the spatially detailed characteristics of the OI algorithm fusing SST data, three statistical parameters of the images are selected for comparing the fused SST image with the original satellite data (MODIS and AMSR-2). In the following, the definition of the image parameters are given.

The mean value (μ) can reflect the average brightness of the image to the human eye, which, if it is moderate, can make an image visually compelling. The variance (δ^2) size is related to the amount of information contained in the image: the larger the variance, the more spread out the image element values are, the more SST values appear in the image, and the more information the data contains. Information entropy (S) quantitatively describes an image's information richness: the larger the information entropy, the richer the information. The equations for these three variables are:

$$\mu = \frac{1}{n} \sum_{i=1}^n x_i \quad (1)$$

$$\delta^2 = \frac{1}{n-1} \sum_{i=1}^n (x_i - \mu)^2 \quad (2)$$

$$S = -c \sum_{i=0}^{L-1} P_i \ln P_i \quad (3)$$

In the above equation, n is the total number of samples, x_i is the i th sample value; c is a constant related to the base of the logarithm, $c = 1 / \log_a 2$, $c = 1$ when $a = 2$, $c = 1 / \ln 2$ when $a = e$, and, in this paper, we use the latter, that is, $c = 1 / \ln 2$. For an individual SST image, it can be considered that the SSTs of its elements are independent of other samples. Then, the SST distribution of this image is $P = \{p_0, p_1, \dots, p_{n-1}\}$, where p_i is the ratio of the SST data with an SST value equal to p_i to the total SST data of the image.

3.3. Comparison Data Processing

3.3.1. Typhoon Data Processing

A total of four typhoons passed through the study area in August 2015, and the typhoons considered in this paper had wind speeds ≥ 24 m/s. The dates on which the daily recorded wind speeds exceeded 24 m/s were considered as affected by typhoons in this paper. Accordingly, the typhoons selected for the study were Typhoon 13 Soudelor (1–8 August, max radius of over 24 m/s winds 180 km), Typhoon 15 Goni (15–26 August, max radius of over 24 m/s winds 220 km), and Typhoon 16 Atsani (16–26 August, max radius of over 24 m/s winds 240 km) (see Figure 2 for detailed paths). In summary, the study area was affected by typhoons for a total of 20 days in August.

3.3.2. Generation of Matching Datasets

The matched datasets for validation must theoretically be synchronized or essentially identical on spatio-temporal scales, but this is in fact difficult to achieve. The four fused remote sensing SST products used in this chapter are all cloud-free, day-by-day data covering the whole sea area, but the spatial resolution of these products varies. In order to facilitate the intercomparison among the fused SST products, this chapter takes the MISST (9 km) with moderate resolution as the standard, and the spatial resolution of other fused SST products is also processed to 9 km by the linear interpolation method. The SST measured by Argo is a single point of data at a certain time. Because the position of an Argo buoy is not fixed, we first take the position of all Argo data in August 2015, and record

the time of the position in days, and then use the date of Argo data as the basis to find the SST fusion product of that time; in space, the coordinates of Argo measurement points were used as the basis, and the fusion products took the average SST values of grid points within a radius of 0.09° from them. A total of 524 OI matches, 522 NOAA OISST matches, 525 MISST sets, and 524 OSTIA matches were finally obtained. The location distribution of each matched data set is shown in Figure 1.

4. Results

4.1. Fusion SST Image Quality Analysis

Currently available SST fusion products primarily employ the OI method. In this approach, fusion error is mainly influenced by the inversion accuracy of the satellite data, the weighting coefficients in the fusion algorithm, and atmospheric conditions. This paper selected MODIS data and AMSR-2 data from the Kuroshio region of the East China Sea for OI fusion, using the OSTIA analysis product as the background field. The fusion process entailed the following steps: (1) vacant SST data of AMSR-2 (shown in Figure 4) after three-day average disposal were provided by the data of the initial background field OSTIA, and (2) the new background field formed by the interpolation of AMSR-2 and OSTIA in turn completed the vacant SST data for MODIS. The daily average results with a spatial resolution of 9 km, which were obtained by fusing SST data from MODIS and AMSR-2 for 15 and 20 August 2015, respectively, using the OI method can be found in Section 4.2.1.

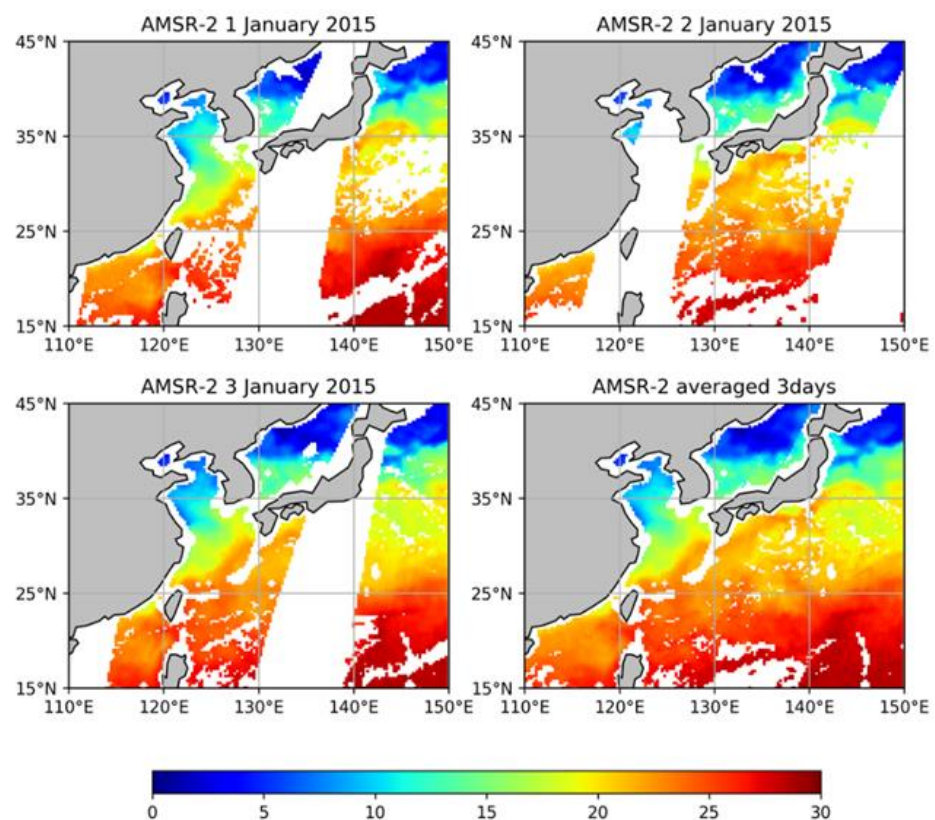


Figure 4. AMSR-2 SST data three-day average processing (SST, colored shading; $^\circ\text{C}$).

To objectively evaluate the quality of the fused SST image using the OI method, this paper compares MODIS SST data, AMSR-2 SST data, and data fused using the OI method based on mean (μ), variance (δ^2) and information entropy of images (S).

Table 1 compares the quality parameters of the three image of MODIS SST, AMSR-2 SST, and SST after OI fusion for 2 January 2015 (as shown in Figure 5). The mean value of the data fused by OI is in the middle, signifying that the visual effect of the fused image is better than that of the single-sensor image. The variance of the three groups of data is

close, indicating that the deviation of the data fused is consistent with that of the original data and that the value of the original data is not changed. The information entropy of the images [28] is a measure of the richness of image information from the information theory perspective, a variable for the objective evaluation of images. The magnitude of information entropy reflects the amount of information carried by the image. The image information entropy of the data fused by OI is the largest, showing that its SST data carries the most information.

Table 1. Comparison of MODIS, AMSR-2, and OI Fusion SST Data Quality Parameters.

Product	Average (°C)	Variance	Entropy
MODIS	19.970	8.513	9.639
AMSR-2	20.094	6.857	11.105
SST-OI	19.535	7.334	11.505

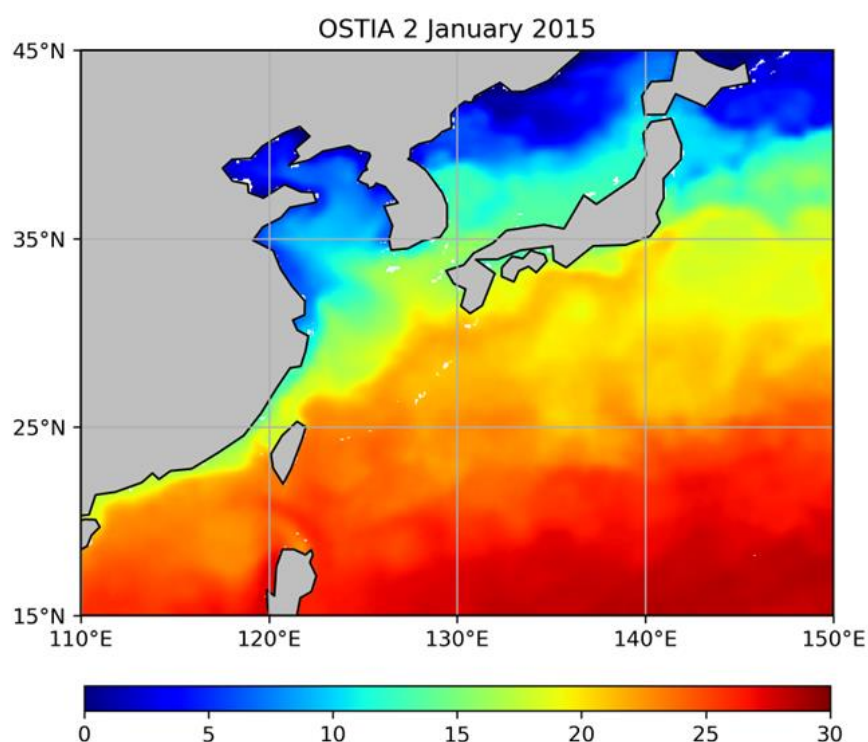


Figure 5. SST fusion result for 2 January 2015 using the OI (SST, colored shading; °C).

4.2. Analysis of Comparative Results

4.2.1. Fusion SST Products Data Distribution

In this paper, the OI algorithm is used to fuse two types of SST data, and the results show that fusion outperforms single sensors. In the future, correcting and improving this algorithm will be of great help to the development of SST fusion products. The following is a comparison of the selected fusion SST products with different SST data, all of which use the OI algorithm.

Figure 6 shows the SST distributions of the four fusion products on 15 August (with typhoon influence) and 20 August (without typhoon influence) 2015, respectively. Qualitative comparison of the single-day SST distributions of each SST fusion product shows that all four fusion products can clearly reflect the single-day SST trends in the Kuroshio region of the East China Sea and are relatively consistent, and the differences in temperature products in the study area are more obvious in the presence of typhoon than in the absence of typhoon influence.

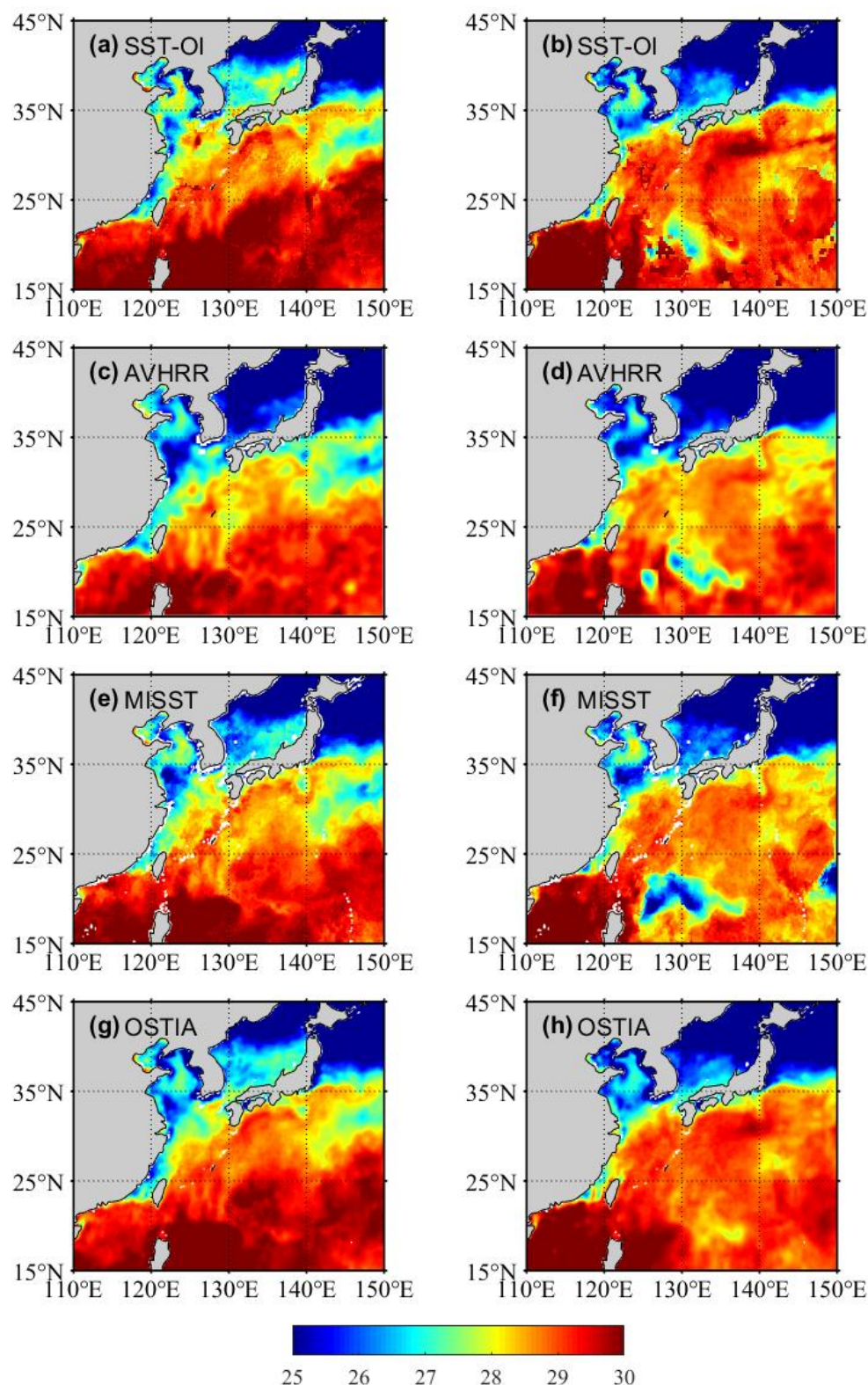


Figure 6. SST distribution of 4 different products in two situations (SST, colored shading; °C). (a) SST-OI product on the 15 August 2015 without typhoon impact, and (b) SST-OI product on the 20 August 2015 affected by typhoon. (c,d), (e,f) and (g,h) as in (a,b), but for AVHRR, MISST, OSTIA product respectively.

4.2.2. Comparison of SST Fusion Results with Argo Data

Table 2 shows the results of the statistical analysis of the SST at the matching points of each of the four fusion products with the Argo buoy, including the number of matching points, mean deviation (Bias), absolute deviation (Abs_Bias), standard deviation (STD), and root mean square error (RMSE). NOAA OISST has a negative deviation of $-0.03\text{ }^{\circ}\text{C}$ from the Argo buoy, MISST has a negative deviation of $-0.04\text{ }^{\circ}\text{C}$ from the Argo buoy, and OSTIA has a positive deviation of $0.04\text{ }^{\circ}\text{C}$ from the Argo buoy. The deviation of MISST is the smallest. An absolute bias of $0.52\text{ }^{\circ}\text{C}$, $0.49\text{ }^{\circ}\text{C}$, $0.45\text{ }^{\circ}\text{C}$, and $0.44\text{ }^{\circ}\text{C}$ for OI, NOAA OISST, MISST, OSTIA, and Argo buoys, respectively; standard deviations of $0.87\text{ }^{\circ}\text{C}$, $0.76\text{ }^{\circ}\text{C}$, $0.69\text{ }^{\circ}\text{C}$ and $0.71\text{ }^{\circ}\text{C}$ for OI, NOAA OISST, MISST, OSTIA, and Argo buoys, respectively. The root mean square errors of OI, NOAA OISST, MISST, OSTIA, and Argo buoys were $0.94\text{ }^{\circ}\text{C}$, $0.76\text{ }^{\circ}\text{C}$, $0.69\text{ }^{\circ}\text{C}$, and $0.71\text{ }^{\circ}\text{C}$, respectively.

Table 2. Statistical analysis of the matching points among four kinds of SST products.

Time	Product	The Number of Matching Points	Bias/ $^{\circ}\text{C}$	Abs_Bias/ $^{\circ}\text{C}$	STD/ $^{\circ}\text{C}$	RMSE/ $^{\circ}\text{C}$
Full month of August 2015	OI	524	0.370	0.525	0.871	0.946
	NOAA OISST	522	-0.028	0.490	0.831	0.831
	MISST	525	-0.040	0.375	0.749	0.749
	OSTIA	524	0.374	0.528	0.932	1.003
With typhoon impact	OI	331	0.364	0.528	0.977	1.041
	NOAA OISST	329	-0.025	0.526	0.944	0.943
	MISST	332	-0.068	0.418	0.880	0.880
	OSTIA	331	0.429	0.566	1.079	1.159
No typhoon impact	OI	193	0.380	0.521	0.652	0.754
	NOAA OISST	193	-0.034	0.428	0.592	0.591
	MISST	193	-0.004	0.303	0.440	0.439
	OSTIA	193	0.279	0.463	0.593	0.654

The day-by-day evolution of the standard deviation in Figure 7 shows that MISST has the least dispersion from Argo and the greatest dispersion from SST-OI and OSTIA; that is, MISST is closer to the actual SST, while the SST-OI and OSTIA products are more different from the actual SST in the case study, especially in the presence of typhoons. Comparing Figure 7 with Table 2, it is found that the fusion results are closer to the Argo SST data on the dates without typhoon influence, and the quality of the OSTIA data is less affected by typhoons, while MISST is more affected by typhoons.

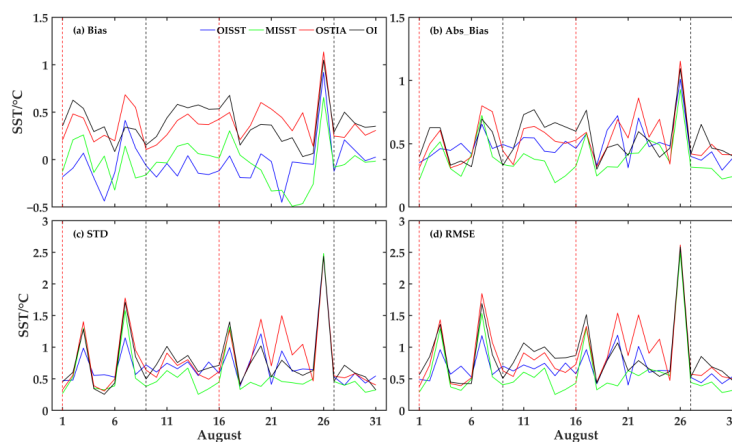


Figure 7. Day-by-day evolution of the statistical analysis of fusion products and Argo buoy SST match points. (a) Average of the mean deviation between the four products at the matching point and the buoy value, (b), (c) and (d) as in (a), but is the mean for absolute deviation, standard deviation, root mean square error respectively. The red vertical line indicates the date when the typhoon started to affect, and the black line indicates the date when the effect ended.

5. Discussion

This investigation applied the OI method to fuse MODIS infrared SST data and AMSR-2 microwave SST data. In addition to combining two data sources in this case, we tested how remote sensing data from other sensors could be merged to meet various needs, with the characteristics of multiple sensor observations combined to obtain an SST fusion product with high spatial and temporal resolution.

We also sought to further improve the accuracy of the fusion results by comparing them with in situ observation data to establish a model, in which in situ data were used to validate the SST data with the measured SST data using the OI method. This approach could also facilitate correcting the SST values by incorporating other factors, such as sea surface wind speed and salinity data. Fusion accuracy could be further improved by adding a vertical correlation model to the OI method.

This paper presented a comparative analysis of the response of the time series fusion products to the typhoon impact in order to evaluate the advantages and disadvantages of the multi-source fusion products before and after the typhoon impact. In addition, the spatial distribution and differences in the analysis results were examined in the Kuroshio region of the ECS.

5.1. Analysis of Fusion Error Sources

Infrared sensors measure the SST depth to the micron, whereas the microwave sensors measure only to the millimeter depth, so that the same area of the SST does not correspond to the same depth. Furthermore, same-depth SST with solar radiation changes daily and the transit times of different sensors are also different, so the data obtained may also be different.

Usually, the OI method performs the calculation and analysis only near the selected points. This approach reduces the computational effort required but can result in a situation in which the analysis results are not optimal for the whole field and can make the fusion results spatially incoherent. Usually, the OI method analyzes only a single variable, which can lead to inconsistency in the physical quantities of the fusion results. In addition, the interpolation calculation itself introduces some noise, which can impact the accuracy of the fused data.

In addition, the reason for the error about the fusion products in this paper may be that better quality control of satellite data is not adopted, for example, the effect of wind speed on SST is not considered, and the SST can be corrected by analyzing the sea surface wind speed and salinity data; it may also be because it is not combined and corrected with the field observation data, and a model can be considered to introduce the measured SST data for correction after OI fusion.

5.2. Analysis of Differences between SST Data and ARGO Buoys

Compared with Argo, the previous study of these L4 products show that OSTIA has the best accuracy among these fusion products, with a standard deviation of its products of less than 0.5 °C [29]. The comparison results of SST data fusion products using the OI algorithm compared in this paper are shown in Table 2 and Figure 6.

Since the SST data of the fusion products are all fully covered, the number of matching points between the four fusion products and the Argo buoy, as well as the number of matching points between the fusion products, is basically the same, and the difference in the coverage of the data itself causes the difference in the number of matching points between each fusion product.

These differences in the comparison of remote sensing fusion SST and buoy SST are related to the mismatch of their observation depths and observation times. The temperature measured by remote sensing SST is generally at the micrometer-mm level at the sea surface, while the buoy SST measures the temperature at a depth of about 1 m. The fused SST calculates the daily average temperature, while the buoy measures the instantaneous kinetic temperature, and these factors make some deviations when comparing the two.

5.3. Analysis of Different SST Data

It has been shown that disregarding the daily warming effect leads to a more significant bias in the fused SST by Martin et al. [30]. The MISST provided by RSS uses the empirical algorithm proposed by Ref. [1] to remove the daily warming effect from the data source in order to reduce the effect of daily variation in SST; the OSTIA has strictly controlled the quality of the daytime SSTs involved in the fusion based on the criterion that the daily warming effect of daytime SSTs is most significant when the wind speed is <6 m/s [31], and the initial field of the SSTs used has eliminated the effect of daily warming.

Figure 5 shows a close distribution of the four SST results in the absence of a typhoon; in the presence of a typhoon, it can be seen that the OSTIA SST is high, especially in the $125\text{--}135^\circ$ E, $18\text{--}20^\circ$ N region, and the rest of the products appear to be significantly colder regions. The reason may be that the response to the typhoon impact is different, and the OSTIA products treat the elimination of daily sea surface warming differently in the data fusion process. It is worth mentioning that MISST does not correct for the base temperature, unlike the two SST fusion products, NOAA OISST and OSTIA, which directly use measured data. However, the AMSR and TMI data have been corrected and validated by buoy data, and the large scale MODIS data bias has been adjusted and corrected by AMSR data.

The results of the statistical analysis in this chapter are in general agreement with the analysis of Martin et al., but the results of the study area fusion data comparison analysis are slightly worse than the global data [30]. The absolute deviation, standard deviation, and root mean square error results show that MISST is slightly better than NOAA OISST and OSTIA, indicating that microwave data provided by microwave sensors can effectively improve the product quality of SST fusion data. Compared with the results of Xi et al. [32,33], we found that the statistical analysis results of the fusion product with Argo are between the statistical analysis results of the two sensors for inversion of SST—better than microwave radiometer and slightly worse than infrared radiometer. This indicates that the fusion product effectively improves the coverage rate through the input of multi-source data and the spatio-temporal smoothing process of the fusion algorithm, which does not reduce the accuracy of the product but also does not significantly improve the product quality.

The statistical analysis results of the matching points of the four fusion products and Argo buoys evolve month-by-month as shown in Figure 6, the change curves are essentially the same, and the data quality is relatively stable. The positive deviation of SST-OI, OSTIA, and Argo buoys is more obvious; the average deviation of MISST is closer to the Argo observation results, and it is observed that the SST-OI product and Argo buoys have obvious positive deviation and fluctuation. This indicates that the product lacks actual measurement data, so it cannot correct for the large scale deviation of remote sensing data and there is a large systematic error, indicating the important role of actual measurement data as input data in the fusion product.

Compared with the Argo buoy, the SST of the four fusion products were all significantly affected by the typhoon, and the average deviation was worse than normal with typhoon effects. The results of the absolute deviation showed that the size of the difference between the four products and Argo was related to the size of the typhoon wind speed and the area affected by the typhoon. The standard deviation and root mean square error evolve month-by-month, showing that in August MISST is slightly better than NOAA OISST and OSTIA, especially in the presence of typhoons. This is due to the fact that in the typhoon region infrared data are missing a lot and MISST with microwave data can improve the quality of the fusion product, further indicating that the quality of the single-sensor NOAA OISST fusion product is significantly affected by changes in cloud coverage. Therefore, SST data from microwave sensors are important when infrared sensors do not provide valid data.

The mean deviation, standard deviation, and root mean square error of the four fusion products on 26 August 2015 are significantly higher than those of other periods of the same month, which may be explained by the fact that this is due to the end of the impact of

typhoon Goni on that day. The impact of Atsani is also mainly not in the area where Argo has data; the SST rises rapidly, the daily SST variation is more variable, and there is a time difference between the products and the SST obtained by the observation. A comparative analysis of the statistical results of the four fusion products with Argo buoys shows that infrared data, microwave data, and real-world data all play an essential role in the fusion products, so that the quality of MISST data, which uses these three types of data, is closer to that of Argo data than that of the SST-OI, NOAA OISST, and OSTIA products.

In Figure 6b, there is an anomaly at 20° N, 129° E (a high SST in the cold vortex), but in Figure 6d,f, there is no anomaly in the cold vortex in the sea, because the SST-OI does not correct for the IR SST anomaly adopting a quality control approach, and the others avoid the anomaly because they have microwave data as input data and different quality control methods, or are corrected with actual measurement data.

The results of Xie et al. [34] demonstrated that in the East China Sea shelf waters with a water depth less than 80 m, the deviation between products increases rapidly with the decreasing water depth, and there are two inflection points with large slopes at water depths of 40 m and 80 m. Therefore, the SST fusion products can be used independently for waters greater than 80 m, but further correction is required near the shore. In this study, because of the small number of Argo in the offshore region, it will not be discussed.

6. Conclusions

This paper investigated and assessed SST using a combination of infrared and microwave data. According to the study findings, the OI method of fusing MODIS and AMSR-2 data in the ECS Kuroshio region on 2 January 2015 yielded more comprehensive spatial coverage and results that were closer to the measured values than the inversion results from single sensor data.

Two approaches are currently available to improve the accuracy of fusion results. This investigation explored the possibility that environmental factors, such as wind speed, might affect the accuracy of SST data. Similarly, the OI method could be used to consider the effect of wind speed and salinity on SST. The other approach, which this study did not investigate, would involve adding a vertical correlation model to the OI method to account for the effect of seawater depth on temperature, which has the potential to significantly increase the fusion effect.

The study applied a bilinear interpolation method to unify the size of the two sets of satellite data when processing the data. However, the selected approach added noise to the data, decreasing the accuracy of the fusion results. Accordingly, a more suitable spatial interpolation method might improve the accuracy of the fusion data.

Our examination encompassed four fusion results that could reflect SST trends in the northwest Pacific Ocean relatively consistently on a spatial scale. In all cases, the standard deviations between the fused data and Argo buoy readings were less than 0.1 °C, and the RMSE was less than 1.1 °C. In contrast, the mean deviation and RMSE of the difference between the fused data and the buoy data were larger when typhoons passed through the study area.

In addition to the OI results, the OSTIA and Argo data demonstrated a large bias under the influence of typhoons, which differed from the conclusions of previous studies that did not consider the influence of typhoons. Consequently, more consideration of the use of OSTIA data in the presence of typhoons is needed. In order to reduce the influence of daily sea surface warming on the fusion results, future applications of the fusion algorithm should aim to eliminate different cases or seek to integrate empirical formulas and filter wind speed data. What is also notable is that the Argo buoys used in this study were farther from shore than those reported in previous studies, which might also have contributed to the bias in the results.

The use of infrared data as part of the input in the data fusion procedure improved the feature resolution and enriched the detailed features of the SST fusion results. Meanwhile, introducing microwave data improved the spatial coverage, compensating for the

influence of clouds on infrared data and reducing the probability of anomalous values. The measured Argo data were able to verify large-scale deviations in SST. Therefore, according to this study's findings, infrared, microwave, and insitu data are all essential elements in producing high-resolution spatial and temporal data and high-precision SST fusion results.

Author Contributions: Conceptualization, J.N. and Y.Z.; methodology, J.N.; software, R.S.; validation, J.N., J.F. and Y.Z.; formal analysis, J.N. and J.F.; investigation, J.F.; resources, R.S.; data curation, J.N.; writing—original draft preparation, J.N.; writing—review and editing, J.F. and Y.Z.; visualization, J.F.; supervision, Y.Z.; project administration, Y.Z.; funding acquisition, Y.Z. All authors have read and agreed to the published version of the manuscript.

Funding: This research was funded by the National Natural Science Foundation (U1901215), the Marine Special Program of Jiangsu Province in China (JSZRHYKJ202007), and the Natural Scientific Foundation of Jiangsu Province (BK20181413).

Data Availability Statement: The MODIS data used for the study are available and downloaded at https://podaac.jpl.nasa.gov/dataset/MODIS_AQUA_L3_SST_THERMAL_DAILY_4KM_Daytime_V2019.0 (accessed on 26 June 2022), AMSR2 data at <https://podaac.jpl.nasa.gov/dataset/AMSR2-REMSS-L3U-v8a> (accessed on 26 June 2022) the ARGO data at <https://data-argo.ifremer.fr> (accessed on 26 June 2022), and typhoon data at tcdata.typhoon.org.cn (accessed on 26 June 2022). In addition, NOAA OISST data can be downloaded at https://podaac.jpl.nasa.gov/dataset/AVHRR_OI-NCEI-L4-GLOB-v2.0 (accessed on 26 June 2022), MISST data at https://podaac.jpl.nasa.gov/dataset/MW_IR_OI-REMSS-L4-GLOB-v5.0 (accessed on 26 June 2022), & OSTIA at <https://podaac.jpl.nasa.gov/dataset/UKMO-L4HRfnd-GLOB-OSTIA> (accessed on 26 June 2022).

Acknowledgments: The data from Hong Kong Observatory, AVISO, and NOAA-CPC are highly appreciated. This research was supported by the National Natural Science Foundation (U1901215), the Marine Special Program of Jiangsu Province in China (JSZRHYKJ202007), and the Natural Scientific Foundation of Jiangsu Province (BK20181413).

Conflicts of Interest: The authors declare no conflict of interest.

References

- Gentemann, C.L.; Donlon, C.J.; Stuart-Menteth, A.; Wentz, F.J. Diurnal signals in satellite sea surface temperature measurements. *Geophys. Res. Lett.* **2003**, *30*, 1140. [[CrossRef](#)]
- Suyu, Y.; Huasheng, Y. Impact of the North and South SSTA in North Pacific on Rainfall Patterns of Flood Season in China. *J. Appl. Meteorol. Sci.* **2007**, *18*, 193–201.
- Xingwei, J.; Mingsen, L.; Jianqiang, L. Satellite ocean exploration of space in China. *Eng. Sci.* **2008**, *6*, 56–62.
- Guan, L.; Kawamura, H. SST availabilities of satellite infrared and microwave measurements. *J. Oceanogr.* **2003**, *59*, 201–209. [[CrossRef](#)]
- Wu, X.R.; Wang, X.D.; Li, W. Review of the application of ocean data assimilation and data fusion techniques. *J. Ocean Technol.* **2015**, *34*, 97–103.
- Bretherton, F.P.; Davis, R.E.; Fandry, C.B. A technique for objective analysis and design of oceanographic experiments applied to MODE-73. *Deep Sea Res. Oceanogr. Abstr.* **1976**, *23*, 559–582. [[CrossRef](#)]
- Carter, E.F.; Robinson, A.R. Analysis models for the estimation of oceanic fields. *J. Atmos. Ocean. Technol.* **1987**, *4*, 49–74. [[CrossRef](#)]
- Reynolds, R.W.; Smith, T.M. Improved global sea surface temperature analyses using optimum interpolation. *J. Clim.* **1994**, *7*, 929–948. [[CrossRef](#)]
- Reynolds, R.W.; Rayner, N.A.; Smith, T.M.; Stokes, D.C.; Wang, W. An improved in situ and satellite SST analysis for climate. *J. Clim.* **2002**, *15*, 1609–1625. [[CrossRef](#)]
- He, R.; Weisberg, R.H.; Zhang, H.; Muller-Karger, F.E.; Helber, R.W. A cloud-free, satellite-derived, sea surface temperature analysis for the West Florida Shelf. *Geophys. Res. Lett.* **2003**, *30*, 1811. [[CrossRef](#)]
- Donlon, C.J. *The GHRSSST-PP Product User Manual, GDS-v1. 5, Rep.*; GHRSSST-PP International Project Office: Exeter, UK, 2005.
- Donlon, C.J.; Martin, M.; Stark, J.; Roberts-Jones, J.; Fiedler, E.; Wimmer, W. The operational sea surface temperature and sea ice analysis (OSTIA) system. *Remote Sens. Environ.* **2012**, *116*, 140–158. [[CrossRef](#)]
- Reynolds, R.W.; Smith, T.M.; Liu, C.; Chelton, D.B.; Casey, K.S.; Schlax, M.G. Daily high-resolution-blended analyses for sea surface temperature. *J. Clim.* **2007**, *20*, 5473–5496. [[CrossRef](#)]
- Thiébaux, J.; Rogers, E.; Wang, W.; Katz, B. A new high-resolution blended real-time global sea surface temperature analysis. *Bull. Am. Meteorol. Soc.* **2003**, *84*, 645–656. [[CrossRef](#)]
- Liu, Y.; Weisberg, R.H.; Law, J.; Huang, B. Evaluation of satellite-derived SST products in identifying the rapid temperature drop on the West Florida Shelf associated with hurricane Irma. *Mar. Technol. Soc. J.* **2018**, *52*, 43. [[CrossRef](#)]

16. O'Carroll, A.G.; Armstrong, E.M.; Beggs, H.M.; Bouali, M.; Casey, K.S.; Corlett, G.K.; Dash, P.; Donlon, C.J.; Gentemann, C.L.; Høyer, J.L.; et al. Observational needs of sea surface temperature. *Front. Mar. Sci.* **2019**, *6*, 420. [[CrossRef](#)]
17. Gentemann, C.L. Three way validation of MODIS and AMSR-E sea surface temperatures. *J. Geophys. Res. Ocean.* **2014**, *119*, 2583–2598. [[CrossRef](#)]
18. Argo Science Team. Argo: The global array of profiling floats. In *Observing the Oceans in the 21st Century*; GODAE Project Office: Melbourne, Australia, 2001; pp. 248–258.
19. Roemmich, D.; Owens, W.B. The ARGO Project: global ocean observations for understanding and prediction of climate variability. *Oceanography* **2000**, *13*, 45–50. [[CrossRef](#)]
20. Notarstefano, G. Argo Float Data and Metadata from Global Data Assembly Centre (Argo GDAC). SEANOE: Silver Spring, MD, USA, 2022. [[CrossRef](#)]
21. Marcello, J.; Eugenio, F.; Hernández, A. Validation of MODIS and AVHRR/3 sea surface temperature retrieval algorithms. In Proceedings of the IGARSS 2004, 2004 IEEE International Geoscience and Remote Sensing Symposium, Anchorage, AK, USA, 20–24 September 2004; Volume 2, pp. 839–842.
22. Ying, M.; Zhang, W.; Yu, H.; Lu, X.; Feng, J.; Fan, Y.; Zhu, Y.; Chen, D. An overview of the China Meteorological Administration tropical cyclone database. *J. Atmos. Ocean. Technol.* **2014**, *31*, 287–301. [[CrossRef](#)]
23. Lu, X.; Yu, H.; Ying, M.; Zhao, B.; Zhang, S.; Lin, L.; Bai, L.; Wan, R. Western North Pacific tropical cyclone database created by the China Meteorological Administration. *Adv. Atmos. Sci.* **2021**, *38*, 690–699. [[CrossRef](#)]
24. Stark, J.D.; Donlon, C.J.; Martin, M.J.; McCulloch, M.E. OSTIA: An operational, high resolution, real time, global sea surface temperature analysis system. In Proceedings of the Oceans 2007-europe, Aberdeen, UK, 18–21 June 2007; pp. 1–4.
25. Donlon, C.; Robinson, I.; Casey, K.S.; Vazquez-Cuervo, J.; Armstrong, E.; Arino, O.; Gentemann, C.; May, D.; LeBorgne, P.; Piollé, J.; et al. The global ocean data assimilation experiment high-resolution sea surface temperature pilot project. *Bull. Am. Meteorol. Soc.* **2007**, *88*, 1197–1214. [[CrossRef](#)]
26. Yocky, D.A. Image merging and data fusion by means of the discrete two-dimensional wavelet transform. *JOSA A* **1995**, *12*, 1834–1841. [[CrossRef](#)]
27. Nunez, J.; Otazu, X.; Fors, O.; Prades, A.; Pala, V.; Arbiol, R. Multi-resolution-based image fusion with additive wavelet decomposition. *IEEE Trans. Geosci. Remote Sens.* **1999**, *37*, 1204–1211. [[CrossRef](#)]
28. Di Renzo, M.; Haas, H. Bit error probability of SM-MIMO over generalized fading channels. *IEEE Trans. Veh. Technol.* **2012**, *61*, 1124–1144. [[CrossRef](#)]
29. Hu, X.; Zhang, C.; Shang, S. Validation and inter-comparison of multi-satellite merged sea surface temperature products in the South China Sea and its adjacent waters. *J. Remote Sens.* **2015**, *19*, 328–338.
30. Martin, M.; Dash, P.; Ignatov, A.; Banzon, V.; Beggs, H.; Brasnett, B.; Cayula, J.F.; Cummings, J.; Donlon, C.; Gentemann, C.; et al. Group for High Resolution Sea Surface temperature (GHRSSST) analysis fields inter-comparisons. Part 1: A GHRSSST multi-product ensemble (GMPE). *Deep Sea Res. Part II Top. Stud. Oceanogr.* **2012**, *77*, 21–30. [[CrossRef](#)]
31. Donlon, C.J.; Robinson, I.S. Observations of the oceanic thermal skin in the Atlantic Ocean. *J. Geophys. Res. Ocean.* **1997**, *102*, 18585–18606. [[CrossRef](#)]
32. Meng, X.; Qingtao, S.; Wenjun, L.; Bin, Z.; Mingsen, L. Intercomparison analysis of merging sea surface temperature products for the Northwest Pacific Ocean. *Haiyang Xuebao* **2016**, *38*, 32–47.
33. Meng, X.; Qingtao, S.; Mingsen, L. Comparison in multi-infrared products of sea surface temperature in northwest pacific. *Oceanol. Limnol. Sin.* **2017**, *48*, 436–453.
34. Xie, J.; Zhu, J.; Li, Y. Assessment and inter-comparison of five high-resolution sea surface temperature products in the shelf and coastal seas around China. *Cont. Shelf Res.* **2008**, *28*, 1286–1293. [[CrossRef](#)]